



Cite this: DOI: 10.1039/d1nj02416g

Visible-light-responsive lanthanide coordination polymers for highly efficient photocatalytic aerobic oxidation of amines and thiols†

 Shuyi An,[‡] Zhifen Guo,[‡] Xin Liu,^a Yan Che,^a Hongzhu Xing^{*,a} and Peng Chen^{*b}

Development of visible-light-induced photocatalytic reactions using molecular oxygen as the terminal oxidant is intriguing in view of the current environmental and energy issues. We report herein the synthesis and characterization of a series of novel photocatalysts of lanthanide coordination polymers (Ln-CPs) with desirable characters of wide-range visible-light adsorption and excellent chemical stability. They show excellent selectivity and yield for the aerobic oxidation of amines and thiols to produce imines and disulphide, respectively. Mechanism studies including electron paramagnetic resonance and radical quenching indicate these Ln-CPs are highly efficient to activate molecular oxygen into highly reactive oxygen species of superoxide radical and singlet oxygen via photoinduced electron and energy transfer, respectively. It is notable that the photocatalytic oxidation of thiols into disulphide have never been reported using a CP photocatalyst prior to this study. Meanwhile, the synthesized CPs exhibits superior photocatalytic performance to other reported ones for amine oxidation due to the synergy of singlet oxygen and superoxide radical species. The work provides an in-depth understanding of the photoinduced oxygen activation based on a CP photocatalyst to accomplish a visible-light-induced reaction, illustrating the great potential of photoactive CPs for green synthesis.

 Received 17th May 2021,
 Accepted 30th July 2021

DOI: 10.1039/d1nj02416g

rsc.li/njc

Introduction

The urgency of energy and environment issues has promoted naturally the rapid development of photocatalysis technology for chemical conversion.^{1–8} Among various photocatalytic reactions, the oxidation of substrates using molecular oxygen as the oxidant has attracted much attention because it is green, cheap and ubiquitous under operation conditions.^{9–15} In particular, this is even more intriguing if the photocatalytic reaction is carried out under visible light irradiation.^{11–15} Previous studies have suggested that molecular oxygen in the triplet state is generally a good acceptor for photoinduced energy transfer (EnT) and/or single electron transfer (SET) in photocatalytic systems, forming highly reactive oxygen species (ROS) such as singlet oxygen (¹O₂), superoxide radical (O₂^{•−}), hydroxyl radical (OH[•]) and others to oxidize various substrates.^{11–20} Furthermore, it is notable that ROS-mediated photocatalytic reactions

usually exhibit excellent selectivity to afford a single product as compared with reactions carried out under heating conditions using molecular oxygen directly.^{21,22}

Coordination polymers (CPs) are crystalline solids constructed by coordination interaction between metal nodes and organic linkers.^{23,24} The intelligent combination of inorganic and organic components affords CPs great structural and functional versatility due to the diversity of metals, linkers and their assembling modes. Nowadays, more and more CPs with narrow band-gap energy have been prepared and explored for photocatalytic reactions under visible light irradiation.^{25–32} Physical measurements and quantum calculation results suggest that they are semiconductor-like materials showing rich charge and energy transfer processes such as metal-to-ligand charge transfer (MLCT), ligand-to-metal charge transfer (LMCT) and ligand-to-ligand charge transfer (LLCT) *etc.*^{33–35} These studies indicate CPs are intriguing candidate for the photoinduced activation of molecular oxygen to trigger oxidative transformation.

We report herein the synthesis of a series of new lanthanide CPs (Ln-CPs) with wide-range visible-light absorption and high chemical stability. The synthesized CPs accomplished efficient photocatalytic performances for the aerobic oxidation of amines and thiols to produce valuable imines and disulphides, respectively. It is notable that the photocatalytic oxidation of thiols into disulphides have never been reported using a CP photocatalyst prior to this study. Meanwhile, the synthesized

^a Laboratory of Advanced Energy Materials, College of Chemistry, Northeast Normal University, Changchun 130021, China. E-mail: xinghz223@nenu.edu.cn

^b Key Laboratory of Functional Inorganic Material Chemistry (MOE), School of Chemistry and Materials Science, Heilongjiang University, Harbin 150080, China. E-mail: jehugu@gmail.com

† Electronic supplementary information (ESI) available: Experimental details, FTIR, TG, PXRD, and crystallographic data. CCDC 2045926–2045928. For ESI and crystallographic data in CIF or other electronic format see DOI: 10.1039/d1nj02416g

‡ These authors contributed equally to this work.

CPs exhibit superior photocatalytic performance to other reported ones for amine oxidation due to the synergy of singlet oxygen and superoxide radical species.

Results and discussion

Synthesis, structure and characterization of Ln-CPs

Crystals of Ln-CPs (Ln = Tb, Ho and Yb) were prepared *via* a solvothermal reaction, where lanthanide nitrate reacts with the aromatic ligand of (4,4'-(anthracene-9,10-diylbis(ethyne-2,1-diyl))dibenzoic acid (ADBEB) in the presence of 2-fluorobenzoic acid and nitric acid (Fig. 1a). For example, the strip-shaped crystals of Tb-CP (named **1Tb**) was prepared by the reaction of $\text{Tb}(\text{NO}_3)_3 \cdot 6\text{H}_2\text{O}$ and ADBEB in *N,N*-dimethylformamide (DMF) at 120 °C for 2 days. Other Ln-CPs of **1Ho** and **1Yb** were prepared under similar conditions but in different molar ratios (see the ESI[†]). As shown in Fig. S1 (ESI[†]), carboxylate ADBEB is chosen here because of its excellent visible light absorption, while the choice of lanthanide ion as metal node is due to the strong coordination interaction between lanthanide ions and carboxylic ligands to afford stable CPs according to the theory of hard and soft acids and bases (HSAB).^{36,37} The prepared crystals were analysed by single-crystal X-ray diffraction, where they show the same framework structure with a general formula of $\text{Ln}(\text{ADBEB})(\text{DMF})(\text{HCOO})$ crystallizing in the monoclinic system $P2_1/c$ space group. The asymmetric unit of the synthesized CP contains one Ln^{3+} , one deprotonated ligand and one DMF molecule, in which the terminal DMF molecule coordinated with Ln^{3+} is disordered showing large anisotropic displacement

parameters (Fig. S2, ESI[†]). As shown in Fig. 1b, each Ln^{3+} ion in octa-coordination mode is connected by four oxygen atoms from four different ADBEB ligands, one oxygen atom from coordinated DMF, and three oxygen atoms from two formate anions. The formate anion should result from the decomposition of DMF during the solvothermal reaction, which has been reported previously for the synthesis of other CP compounds.^{38,39} The bond lengths of the Tb–O bond in **1Tb** are from 2.274(4) to 2.615(4) Å. The Ln–O bond lengths in **1Ho** and **1Yb** are in the range of 2.262(4)–2.602(4) Å and 2.226(3)–2.621(3) Å, respectively. These values match well with those reported for other Ln-CPs.^{40,41} Adjacent lanthanide ions are connected by $\text{u}_3\text{-O}$ atoms from formate to form dimers containing Ln–O–Ln binding (Fig. 1b and c). The dimers are further interlinked by carboxylate groups from ADBEB to generate a two-dimensional framework (Fig. 1c and d). The anthracene chromophores on ADBEB in the framework are in parallel arrangement with a face-to-face distance of *ca.* 3.637 Å (Fig. S2d, ESI[†]).

The crystalline powders of Ln-CPs were studied by powder X-ray diffraction where the experimental patterns fit well with the simulated one, suggesting the prepared samples are in good purity (Fig. 2a). Fourier transformed infrared (FTIR) spectra of the Ln-CPs were further measured at room temperature (Fig. S3, ESI[†]). Absorption peak at *ca.* 2195 cm^{-1} on the spectra is attributed to the characteristic stretching vibration of the ethynyl group on the ADBEB ligand. Absorption at *ca.* 862, 787 and 761 cm^{-1} can be ascribed to the out-of-plane vibration of C–H bonds on the benzene groups of ADBEB. Intense peaks at *ca.* 1575 and 1410 cm^{-1} are due to the vibrations of carboxylate groups.⁴² A series of weak peaks from 2853 to 3060 cm^{-1} should

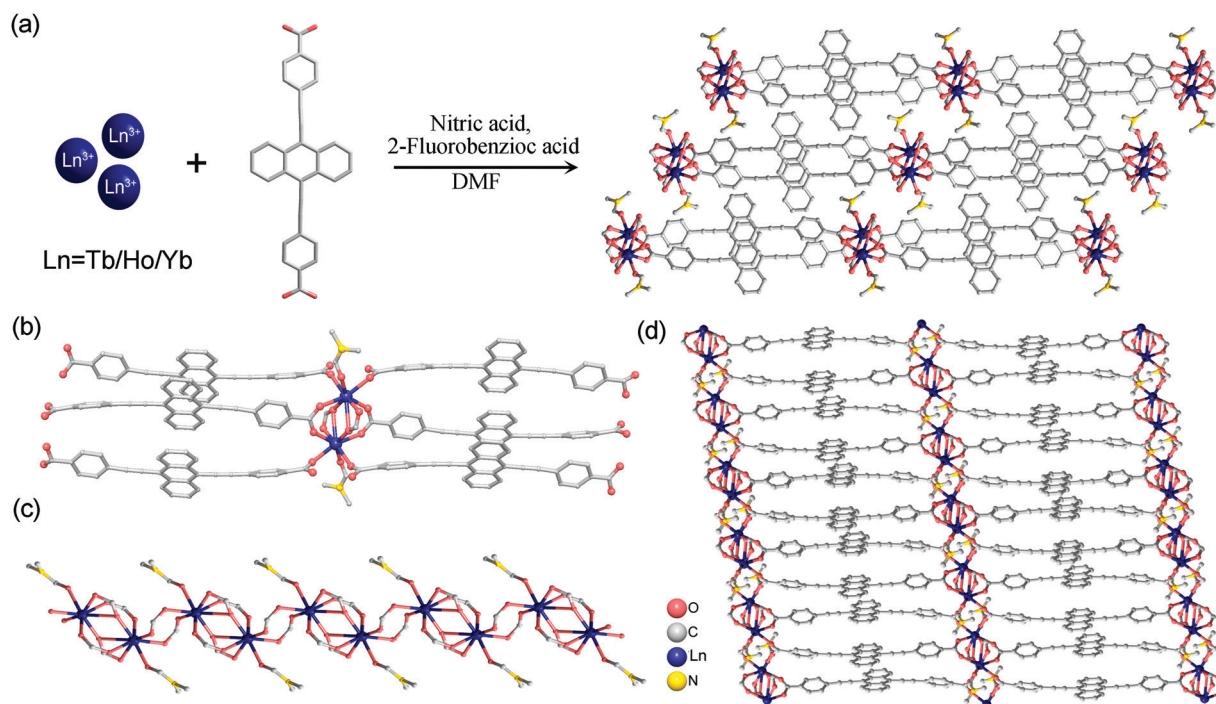


Fig. 1 (a) Solvothermal synthesis of Ln-CPs in a two-dimensional structure. (b) Coordination between lanthanide ions and ADBEB ligand. (c) Chain-like unit containing dimers of lanthanide ions. (d) A single layer in the structure of Ln-CPs. All hydrogen atoms are omitted for clarity.

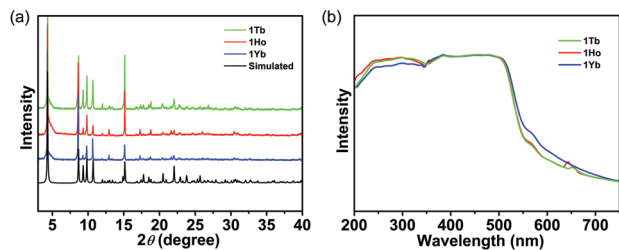


Fig. 2 (a) PXRD patterns of Ln-CPs. (b) UV-vis spectra of Ln-CPs.

be associated with the DMF molecule in the structure.⁴³ Thermogravimetric (TG) analysis showed that these Ln-CPs exhibit very similar thermal behaviour displaying three-step weight loss (Fig. S4, ESI[†]). The first weight loss of 10.93% (**1Tb**, calcd: 9.86%), 12.08% (**1Ho**, calcd: 9.78%) and 10.28% (**1Yb**, calcd: 9.69%) occurs at 210 °C, corresponding to the removal of the DMF molecule coordinated with a lanthanide ion. The next weight loss of 5.83% (**1Tb**, calcd: 5.94%), 5.65% (**1Ho**, calcd: 5.86%) and 5.85% (**1Yb**, calcd: 5.83%) at 350 °C should be related to the removal of coordinated formate groups. The last weight loss of 59.69% (**1Tb**, calcd: 62.70%), 61.72% (**1Ho**, calcd: 62.10%) and 58.02% (**1Yb**, calcd: 61.49%) started at *ca.* 440 °C is attributed to the decomposition of the organic ligand in Ln-CPs.

Solid state UV-vis spectra of the prepared Ln-CPs exhibit wide-range absorption in the visible light region up to 650 nm (Fig. 2b). The intense adsorption of Ln-CPs at 400–520 nm should originate from the transition absorption of conjugated ADBEB in the structure (Fig. S1, ESI[†]). The band gap energy of these Ln-CPs is evaluated according to the energy dependence relationship of $\alpha h\nu = (h\nu - E_g)^{1/2}$, where α and E_g are the absorption coefficient and the energy gap of a semiconductor, respectively.⁴⁴ The plot of $(\alpha h\nu)^2$ versus photon energy ($h\nu$) is fitted linearly, and the band-gap energies of Ln-CPs were estimated to be *ca.* 2.04 eV (**1Tb**), 2.05 eV (**1Ho**) and 2.25 eV (**1Yb**), respectively (Fig. S5, ESI[†]). The excellent optical property of the synthesized CPs suggests they might be promising photocatalysts to activate molecular oxygen, which is further explored using **1Tb** as a representative photocatalyst.

Photocatalytic aerobic oxidation of amines

Imines with active C=N bonds are variable reaction intermediates that can carry out reactions such as reduction, addition and cycloaddition, playing an important role in the synthesis of pharmaceuticals and functional materials.⁴⁵ The direct photocatalytic synthesis of imine *via* aerobic oxidation of amine substrate was then explored using **1Tb** as the photocatalyst. At the very start, the chemical stability of **1Tb** in different solvents was tested. PXRD studies suggested that **1Tb** is stable enough when it was soaked in organic solvents such as DMF, EtOH, MeCN and CHCl₃ for 24 hours (Fig. S6, ESI[†]). Thereafter, visible-light-induced photocatalytic oxidation of the model substrate of benzylamine was examined. At first, the photocatalytic reaction was carried out by exploring the optimal solvent under an oxygen atmosphere (Table S2, ESI[†]). The

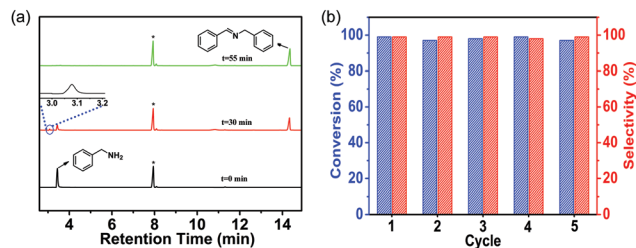


Fig. 3 (a) GC signals for photocatalytic aerobic oxidation of benzylamine at different reaction times. The inset shows the occurrence of aldehyde intermediate and the asterisk designates internal standards of biphenyl. (b) Cycling experiments of photocatalytic amine oxidation over **1Tb**.

conversion and selectivity of amine was detected by GC with biphenyl as the internal standard (Fig. 3a), and the product formation *versus* reaction time under optimized conditions is shown in Fig. S7 (ESI[†]).

Preliminary experiments suggest an oxidation reaction in a mixture of DMF/dioxane (V/V = 1/1) gave an ideal performance where the raw amine transformed into imine within 60 minutes in excellent yield (99%). The turnover frequency (TOF) is calculated to be 13378 $\mu\text{mol g}^{-1} \text{h}^{-1}$. It is remarkable that **1Tb** exhibits a superior catalytic performance for amine oxidation than reported CP photocatalysts of NH₂-MIL-125(Ti), PCN-222 and others (Table S3, ESI[†]).^{28,30,46–49} Control experiments suggest that the presence of **1Tb** and visible light is indispensable for the reaction (Table 1, entries 2 and 3). The ADBEB linker shows evident visible-light adsorption (Fig. S1, ESI[†]), indicating that the photocatalytic reaction of CP mainly relies on the photoactive linker (Table 1, entry 4). However, no photocatalytic product of imines was collected when using lanthanide metal salts of Tb(NO₃)₃, Ho(NO₃)₃ or Yb(NO₃)₃ as the catalyst alone under optimized conditions.

Table 1 Photocatalytic oxidation of benzylamine over **1Tb** under visible light

Entry	Variation from the standard conditions ^a	Con. ^b (%)	Sel. ^c (%)
1	None	99	99
2	None 1Tb	25	95
3	None light	5	99
4	ADBEB	70	95
5	N ₂	5	99
6	Air	31	99
7 ^d	BQ	59	99
8 ^e	DABCO	43	99
9 ^f	AgNO ₃	24	99
10 ^g	TEOA	48	99

^a Reaction condition: benzylamines: 0.2 mmol, **1Tb**: 7.4 mg, biphenyl: 0.1 mmol, solvent: DMF/dioxane (1 mL, V/V, 1:1), O₂ atmosphere, visible light irradiation for 60 min. ^b Determined by GC. ^c Determined by GC. ^d 0.2 mmol BQ was added as the superoxide radical quenching agent. ^e 0.2 mmol DABCO was added as the singlet oxygen quenching agent. ^f 0.2 mmol AgNO₃ was added as the electron quenching agent. ^g 0.2 mmol TEOA was added as the hole quenching agent.

Only a trace amount of substrate was converted to imine (5%) if the reaction was carried out under nitrogen instead of oxygen (Table 1, entry 5). When the reaction was performed under an air atmosphere, the yield was 31% (Table 1, entry 6). Results suggest molecular oxygen is important for the reaction. In addition, the reusability of photocatalyst **1Tb** was investigated, where it can be recycled by centrifugation and showed good stability in the cycling reactions (Fig. 3b and Fig. S8–S10, ESI†). Other Ln-CPs of **1Ho** and **1Yb** have also been studied for the reaction. They show excellent reaction selectivity (99%) and comparable conversion rate as that shown by **1Tb** (Fig. 6). ICP-AES measurements showed that the lanthanide ions in CPs did not leach into solution after photocatalytic oxidation of amines, indicating the prepared CPs are as stable as other Ln-CPs used in photocatalytic reactions.^{50–56}

The scope of amine substrates was surveyed under optimized conditions. As shown in Table 2, various benzylamine derivatives exhibit excellent selectivity (>99%) to generate corresponding imines *via* photocatalytic reaction at room temperature. Nonetheless, the conversion efficiencies of the reactions are different from each other. For methyl-substituted derivatives on the phenyl group of benzylamine, the conversion rate is in the order of *ortho*- > *meta*- > *para*-substitution (entries 1–3), indicating that the steric effect plays an important role for the reaction. This has also been verified by substrates with fluorine groups (entries 5–7). For derivatives with electron-withdrawing groups of halides on the *para*-position, the

Table 2 Visible-light-induced photocatalytic oxidation of amines over **1Tb**^a

Entry	R	Products	T (min)	Con. ^b (%)	Sel. ^c (%)	Yield ^d (%)
1	<i>o</i> -CH ₃		50	99	99	96
2	<i>m</i> -CH ₃		60	99	99	97
3	<i>p</i> -CH ₃		105	99	99	95
4	<i>p</i> -OCH ₃		75	99	99	95
5	<i>o</i> -F		75	99	99	98
6	<i>m</i> -F		70	99	99	94
7	<i>p</i> -F		60	99	99	97
8	<i>p</i> -Cl		65	99	99	97
9	<i>p</i> -Br		70	99	99	95

^a Reaction condition: 0.2 mmol amines, 7.4 mg **1Tb**, DMF/dioxane (1 mL, V/V = 1:1), 0.1 mmol biphenyl, O₂ atmosphere under visible light irradiation. ^b Determined by GC. ^c Determined by GC. ^d Isolated yield.

conversion rate is in the order of fluoro- > chlorine- > bromo-derivative (entries 7–9), indicating that the electronic effect should also be important for the reaction.

Reaction mechanism of amine oxidation

The mechanism of photocatalytic aerobic oxidation of amines over **1Tb** was studied. As mentioned above, the photoinduced energy/electron transfer from CPs to molecular oxygen would lead to the formation of various ROS in the reaction potentially. This was investigated first by quenching experiments. Typical quenchers of benzoquinone (BQ) and triethylenediamine (DABCO) were employed equivalently in the reaction to capture O₂^{•-} and ¹O₂ respectively. As shown in Table 1 (entries 7 and 8), the conversion of amine decreased moderately to 59% (BQ) or 43% (DABCO) upon the addition of these quenchers, indicating that both O₂^{•-} and ¹O₂ should be the ROS in the reaction. However, the former depends primarily on electron transfer and the latter relies on energy transfer of the excited Ln-CPs.

Visible-light-induced activation of molecular oxygen by **1Tb** *via* electron transfer was then investigated. Firstly, the photo-generation charge of **1Tb** was studied by transient photocurrent measurement. The photocurrent response of **1Tb** has been recorded with a three-electrode system in 0.2 M Na₂SO₄ solution. As shown in Fig. 4a, **1Tb** exhibits an intense and reproducible photocurrent signal upon visible light irradiation, indicating the generation of charge carriers due to electron-hole separation. The subsequent electron transfer to triplet oxygen forming O₂^{•-} species was detected by electron paramagnetic resonance (EPR) measurements (Fig. 4b). A typical capture agent of 5,5-dimethyl-1-pyrroline *N*-oxide (DMPO) was added in the suspension of **1Tb** in dioxane to capture O₂^{•-} where a xenon lamp (500 W) was used to provide *in situ* visible light irradiation under EPR settings (see the Experimental section). At first, a weak EPR signal was detected under dark

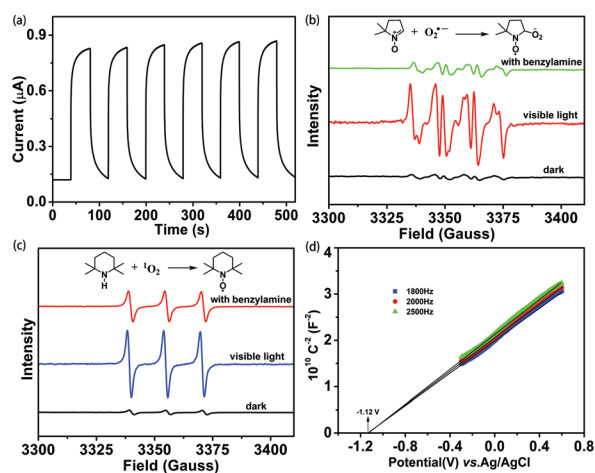


Fig. 4 (a) Photocurrent measurement of **1Tb** in 0.2 M Na₂SO₄. (b) EPR spectrum of the superoxide radical using DMPO as a trapping agent under different conditions. (c) EPR spectrum of singlet oxygen using TEMP as the trapping agent under different conditions. (d) Mott–Schottky plots of **1Tb** in 0.2 M Na₂SO₄.

conditions. Thereafter, intensive EPR signals corresponding to the generation of DMPO- $O_2^{\bullet-}$ adduct occurred after visible light irradiation,³⁰ suggesting clearly the formation of superoxide species owing to the electron transfer from excited **1Tb** to oxygen molecules. The occurrence of a weak EPR signal under dark conditions should be due to the inevitable visible-light illumination of **1Tb** during the sample preparation. Subsequently, the addition of substrate decreases the EPR signal obviously, and suggests a strong interaction between amine and $O_2^{\bullet-}$. The generation of superoxide radical *via* photoinduced electron transfer can also be verified by adding electron sacrificial agent of $AgNO_3$ into the photocatalytic reaction (Table 1, entry 9). The result suggests the target transformation has been quenched dramatically due to the addition of an alternative electron acceptor.

Photoinduced oxygen activation *via* energy transfer to form reactive singlet oxygen was also studied by EPR measurement. A singlet oxygen trapping agent of 2,2,6,6-tetramethyl-4-piperidone (TEMP) was added into a suspension of **1Tb** during EPR tests. As shown in Fig. 4c, a weak EPR response was detected under dark conditions, owing to the generation of a small amount of 1O_2 which was captured by TEMP during sample preparation. Upon *in situ* visible light irradiation, the EPR response increases significantly due to the continuous generation of 1O_2 . Further addition of amine substrate quenches the EPR response, indicating the direct reaction between amine and 1O_2 . These results suggest clearly the photoinduced generation of 1O_2 in the photocatalytic system. Hence, it is clear that a synergy of 1O_2 and $O_2^{\bullet-}$ takes responsibility for the photocatalytic oxidation of amine into imine.

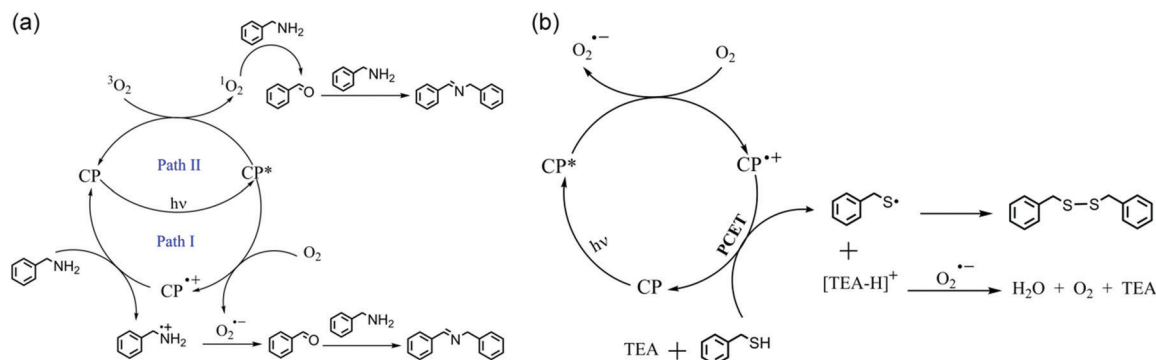
The redox potential of the CP was then studied to further understand its photocatalytic performance on amine oxidation. Mott-Schottky plots were measured at different frequencies where a positive slope of C^2 values *versus* potential has been observed, indicating the n-type semiconductor behaviour of **1Tb** (Fig. 4d and Fig. S11, ESI†).^{57,58} The measured plots intersect at -1.12 V *versus* Ag/AgCl electrode, *i.e.* -0.92 V *versus* normal hydrogen electrode (NHE). In view that the measured flat-band potential of an n-type semiconductor is usually 0.1 V lower than its conduction band (CB), hence the CB of **1Tb** would be *ca.* -1.02 V *versus* NHE. The reduction potential (CB)

of **1Tb** is more negative than $E(O_2/O_2^{\bullet-})$ (-0.33 V *vs.* NHE),³⁰ suggesting that the activation of molecular oxygen into superoxide radical by **1Tb** is thermodynamically feasible. The valence band (VB) of **1Tb** was calculated to be $+1.02$ V *versus* NHE. This value is more positive than that of benzylamine ($+0.76$ V *vs.* NHE), indicating the direct oxidation of amine by holes on **1Tb**. This has been studied by the photocatalytic reaction using a hole sacrificial agent of triethanolamine (TEOA). The experiment shows that the amine oxidation was significantly suppressed due to the addition of TEOA (Table 1, entry 10), confirming the direct oxidation of amine substrate by excited **1Tb**.

Based on these findings, a plausible reaction mechanism is proposed in Scheme 1a. According to the reported studies and our results, the reaction may experience a possible pathway where the oxidation of amine leads to the formation of aldehyde, followed by a condensation reaction to generate imine product.^{11,16,29} This has been confirmed by the detection of the intermediate of benzaldehyde during the reaction (Fig. 3a, inset). And a direct interaction between amine substrate and reactive oxygen species has been verified by EPR studies where both EPR signals of $O_2^{\bullet-}$ and 1O_2 have been quenched significantly upon the addition of amine (Fig. 4b and c).

Photocatalytic aerobic oxidation of thiols

The successful oxidation of amines using **1Tb** as a photocatalyst inspires our search of other photocatalytic aerobic reactions, such as the oxidative coupling of thiols to disulphide. Disulphide bonds are very important in nature since they are essential for proteins and peptides to fold into their biologically active conformation.^{59,60} The formation of disulphide is also a matter of interest because they are valuable anti-oxidants, pharmaceuticals pesticides and rubber vulcanization reagents.⁶¹⁻⁶³ The formation of these chemicals can be accomplished by various oxidants such as permanganates, chromium peroxide and sodium perborate, as well as metal catalysts.⁶⁴⁻⁶⁷ The increasing environmental concerns associated with the use of toxic and dangerous oxidants guides people to develop oxidation methodologies using molecular oxygen as the oxidant. Prior to this study, the aerobic oxidation of thiols to disulphide has been achieved using Fe-CP as a solid redox catalyst at 70 °C.⁶⁸ However, the oxidative dimerization of thiols



Scheme 1 Plausible mechanism for photocatalytic aerobic oxidation of amine and thiol over Ln-CPs.

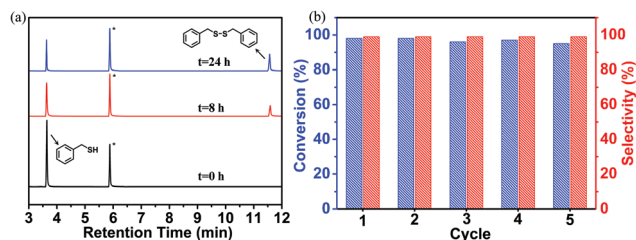


Fig. 5 (a) GC signals for thiol oxidation at different reaction times. Asterisk designates the internal standard of biphenyl. (b) Cycling experiments of photocatalytic aerobic oxidation of thiol over **1Tb**.

based on CP-mediated photocatalytic reaction has been rarely studied until now.

Visible-light-induced aerobic oxidation of thiols using **1Tb** as the photocatalyst was carried out under room temperature. The reactions were monitored by GC with biphenyl as the internal standard (Fig. 5a and Fig. S12, ESI†). As shown in Table 3, a series of control experiments suggest that visible light, photocatalyst **1Tb** and oxygen are important for the reaction (entries 1–5). The photocatalytic reaction gave a high selectivity (99%) and moderate conversion (57%) of thiol into disulfide at 24 hours in the solvent of DMF/MeCN (V/V = 4/1) (Table 3, entry 1 and Table S4, ESI†). The organic ligand of ADBEB exhibited 35% yield of disulphide (Table 3, entry 6), and the lanthanide metal salts of Tb(NO)₃, Ho(NO)₃ or Yb(NO)₃ as catalyst alone were almost no disulphide products, indicating the photo-responsive ligand plays a significant role on the reaction.

According to previous reports of aerobic dimerization of thiols, the addition of an organic base of triethylamine (TEA)

Table 3 Photocatalytic oxidation of thiol over **1Tb** under visible light^a

Entry	Reaction conditions ^a	Con. ^b (%)	Sel. ^c (%)
1	Standard	57	99
2	Without 1Tb	15	90
3	Without light	0	—
4	N ₂ instead of O ₂	14	93
5	Air instead of O ₂	31	99
6	ADBEB	35	99
7 ^d	With TEA	99	99
8 ^e	With BQ	2	99
9 ^f	With DABCO	56	99
10 ^g	With IPA	54	99
11 ^h	AgNO ₃	8	99
12 ⁱ	KI	18	99

^a Scale of reaction: benzyl thiol (0.2 mmol, 23 μL), **1Tb** (7.4 mg), DMF/MeCN (1 mL, V/V = 4:1), visible light, 24 hours under an O₂ atmosphere. ^b Determined by GC with biphenyl as an internal standard.

^c Determined by GC with biphenyl as an internal standard. ^d 0.2 mmol TEA (triethylamine) was added with visible light irradiation for 8 hours.

^e 0.2 mmol BQ was added as the superoxide radical capture agent.

^f 0.2 mmol DABCO was added as the singlet oxygen capture agent.

^g 0.2 mmol isopropanol (IPA) was added as the hydroxyl radical capture agent.

^h 0.2 mmol AgNO₃ was added as the electron quenching agent.

ⁱ 0.2 mmol KI was added as the hole quenching agent.

Table 4 Visible-light induced photocatalytic oxidation of thiols over **1Tb**^a

R—SH		$\xrightarrow[\text{DMF/MeCN, O}_2, \text{TEA}]{\text{1Tb, visible light}}$		R—S—S—R		
Entry	R	Products	T (h)	Con. ^b (%)	Sel. ^c (%)	Yield ^d (%)
1	PhCH ₂		8	99	99	98
2	<i>p</i> -OCH ₃ PhCH ₂		11	99	99	95
3	<i>p</i> -FPhCH ₂		7	99	99	96
4	<i>p</i> -ClPhCH ₂		7	99	99	95
5	CH ₃ OOCCH ₂		6	99	99	97
6	<i>n</i> -Butane		12	99	99	93
7	<i>n</i> -Octyl		12	67	99	62
8	Cyclohexyl		12	40	99	42

^a Reaction condition: thiol: 0.2 mmol, **1Tb**: 7.4 mg, solvent: DMF/MeCN (1 mL, V/V, 4:1), TEA: 0.2 mmol, O₂ atmosphere under visible light irradiation. ^b Determined by GC. ^c Determined by GC. ^d Isolated yield.

would enhance the reaction significantly.^{17,69–73} The experiment shows the addition of TEA had a significant influence on the conversion rate (Table 3, entry 7) in **1Tb**-mediated reaction. The full transformation of substrate into disulphide could be achieved within 8 hours in the presence of TEA in stoichiometric quantity. The turnover frequency (TOF) is calculated to be 1672 μmol g⁻¹ h⁻¹.

The compatibility of **1Tb**-mediated reaction under optimized conditions was explored by employing a series of thiols with various functional groups (Table 4). Experiments showed that thiols including thiol derivatives and aliphatic ones were successfully transformed into disulphide with excellent selectivity (99%). However, an obvious difference of reaction rate between these substrates was observed. For thiol derivatives, the conversion of substrates substituted with electron-withdrawing F/Cl groups are much more rapid than that substituted with electron-donating methoxy group (Table 4,

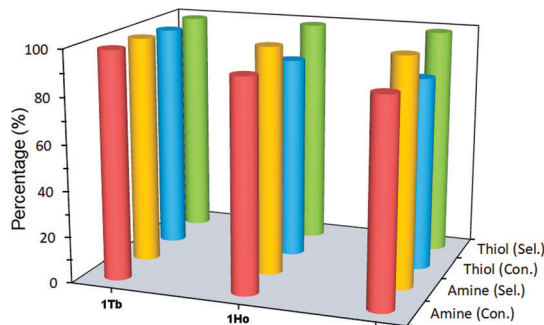


Fig. 6 Photocatalytic aerobic oxidation of amine and thiol over Ln-CPs under visible light irradiation.

entries 2–4), indicating that the electronic effect of the substrate plays an important role on the reaction. The electronic effect can also be evidenced by the rapid reaction of thiol modified with an electron-withdrawing ester group (Table 4, entry 5). Other thiols with aliphatic and cyclohexyl groups have also been studied to be effective for the selective synthesis of disulphide (Table 4, entries 6–8).

Thereafter, we extended the reaction towards reusability of **1Tb**, where its photocatalytic activity was maintained within five cycles (Fig. 5b and Fig. S13–S15, ESI†). Other Ln-CPs of **1Ho** and **1Yb** also show excellent reaction selectivity (99%) but lower substrate conversion (Fig. 6). ICP-AES measurements showed there are no detectable lanthanide ions in the solution after the photocatalytic reaction, proving the good stability of the synthesized coordination polymers for photocatalytic application.

Reaction mechanism of thiol oxidation

To investigate the reaction mechanism, a number of control experiments were studied (Table 3 and Table S5, ESI†). It is confirmed that the oxidation of thiol to disulphide was significantly inhibited by a superoxide radical scavenger, BQ (2% yield), whereas the addition of a singlet oxygen scavenger, DABCO, had no effect on the reaction. In addition, the use of a hydroxyl radical scavenger, isopropanol (IPA), was also unable to quench the reaction. These experiments indicate that an $O_2^{\bullet-}$ radical rather than singlet oxygen or hydroxyl radical serves as the primary ROS in the system. Photoinduced electron transfer from **1Tb** to generate a superoxide radical has been studied using a competitive electron sacrificial agent of $AgNO_3$. The photocatalytic experiment shows the reaction has been quenched significantly when $AgNO_3$ was added (Table 3, entry 11), indicating that the target reaction depends heavily on the photoinduced electron transfer to generate superoxide radicals. In addition, experiments using the hole sacrificial agent of KI also gave a quenched reaction with low performance, indicating the oxidative hole on **1Tb** plays an important role on the reaction (Table 3, entry 12).

On the basis of our experiments and previous reports, a plausible mechanism involving a concerted transfer of an electron and a proton for the aerobic reaction of thiols is depicted in Scheme 1b. Under visible light irradiation, **1Tb** activates molecular oxygen into $O_2^{\bullet-}$ via a single electron transfer process. The resulting hole on **1Tb** oxidizes the reductive substrate of thiol to generate thiyl radical providing a disulphide product via rapid dimerization reaction, in which the reaction is accompanied with a proton transfer process forming H_2O and O_2 . The proposed proton-coupled electron transfer (PCET) mechanism has been evidenced by the experiment using an organic base to accelerate the reaction. The photocatalytic experiment shows the addition of TEA promotes the catalytic performance dramatically. The same trend has also been observed for photocatalytic aerobic oxidation of thiols using other photocatalysts via a PCET mechanism.^{17,69,70} In view that the oxidation potential of TEA (+1.19 V vs. NHE)^{74,75} is more positive than **1Tb** (+1.02 V vs. NHE), TEA might serve as a weak base catalyst to abstract a proton from the thiol substrate (+0.7 V vs. NHE)

generating thiolate (+0.306 V vs. NHE)^{76,77} which is more easily oxidized by **1Tb**, thereby improving the photocatalytic performance.

Conclusions

In summary, this manuscript reports the synthesis of a series of novel visible-light-respective lanthanide CPs in a two-dimensional framework. Studies suggest they are ideal sensitizers to activate molecular oxygen via photoinduced energy and electron transfer processes to generate highly reactive oxygen species of singlet oxygen and superoxide radical, thus showing a high conversion rate and excellent reaction selectivity for the oxidation of amines and thiols. Studies show lanthanide CP-mediated aerobic oxidation of amines into imines relies on the synergy of singlet oxygen and superoxide radicals to produce an aldehyde intermediate; while the same reactive oxygen species, of the superoxide radical, is involved in the proton-coupled electron transfer process to generate disulphide from the thiol substrate. The work provides an in-depth understanding for the rational utilization of a CP photocatalyst to accomplish visible-light-induced organic transformation under the guidance of green chemistry.

Experimental section

Synthesis of lanthanide CPs

The crystals of lanthanide CP **1Tb** were synthesized by solvothermal reaction. Typically, $Tb(NO_3)_3 \cdot 6H_2O$ (0.52 mmol, 0.242 g) and organic ligand ADBEB (0.13 mmol, 60 mg) were mixed in DMF (7.5 mL), then 2-fluorobenzoic acid (5 mmol, 0.7 g) and nitric acid (3 M, 1.5 mL) were added into the mixture as modulators. Thereafter, the mixture was sealed in a 15 mL Teflon-lined stainless autoclave maintained at 120 °C for 48 hours, and then cooled to room temperature naturally. The synthesized strip-shaped crystals in red colour were collected and washed with fresh DMF and ethanol three times. Yield: 63.5% based on an organic linker.

1Ho and **1Yb** were prepared by a solvothermal method like **1Tb**. A mixture of lanthanide nitrate hexahydrate (0.52 mmol), organic ligand ADBEB (0.13 mmol, 60 mg), 2-fluorobenzoic acid (5 mmol, 0.7 g) and nitric acid (0.3 M, 1 mL) in DMF (7.5 mL) was placed into a Teflon autoclave and heated to 120 °C for 2 days. The yields of **1Ho** and **1Yb** are 75.3% and 77.2% based on ligand, respectively. These compounds possess isomorphic structures. This has been further confirmed by the single-crystal X-ray diffraction (SCXRD) data in Table S1 (ESI†).

Photocatalytic reactions of amines

Photocatalytic oxidation of amines was conducted at room temperature. Typically, Ln-CP (0.01 mmol, 5 mol%) and benzylamine (0.2 mmol, 22 μ L) was placed in a vial (4 mL) with a mixed solvent of dioxane/DMF (1 mL, V/V, 1 : 1), where biphenyl (0.1 mmol, 15.4 mg) was added as the internal standard. Then the mixture was stirred magnetically under an O_2 atmosphere and irradiated by a 300 W xenon lamp where UV and IR filters

were used to remove light less than 420 nm and larger than 800 nm. A small number of reaction suspension was fetched out at fixed time intervals, the suspension was filtered with a porous membrane (22 μm in diameter) and injected into GC. The products were identified by standard chemicals. The isolated yields of the products are provided in Table 2 and the ^1H NMR data are provided in the ESI.†

Photocatalytic reactions of thiols

Typically, Ln-CP (0.01 mmol, 5 mol%) and a mixed solvent of DMF/MeCN (1 mL, V/V, 4 : 1) were placed in a vial (4 mL), where diphenyl (0.1 mmol, 15.4 mg) was added as the internal standard. Benzyl thiol (0.2 mmol, 23 μL) and TEA (0.2 mmol, 28 μL) were injected by syringe. Then the mixture was irradiation by a 300 W xenon lamp under an O_2 atmosphere, where UV and IR filters were used to remove lights less than 420 nm and larger than 800 nm. The products were identified by standard chemicals. The isolated yields of the products are provided in Table 4 and the ^1H NMR data are provided in the ESI.†

Electron paramagnetic resonance (EPR) measurements

The photoinduced generation of reactive oxygen species (ROS) and the interaction between ROS and substrate was studied by EPR detection. A xenon lamp (500 W) was used to provide *in situ* visible-light irradiation where UV and IR filters were used to remove lights less than 420 nm and larger than 800 nm. Chemicals of 5,5-dimethyl-1-pyrroline-*N*-oxide (DMPO) and 2,2,6,6-tetramethylpiperidine (TEMP) was used as the EPR tapping agent for the detection of superoxide radical and singlet oxygen, respectively. Typically, a mixture of Ln-CP and DMPO/TEMP was added in MeCN (oxygen saturated), and then the EPR signal under dark conditions and under visible light illumination was detected. Then the substrate of benzylamine (0.2 mmol, 22 μL) was added into the system to study the interaction between the ROS and substrate.

Author contributions

Hongzhu Xing, Zhifen Guo and Shuyi An designed the overall methodology and experimental idea; Zhifen Guo, Xin Liu, Shuyi An and Yan Che completed the experiments and characterizations together; Zhifen Guo and Hongzhu Xing analysed and discussed the data; Hongzhu Xing and Peng Chen wrote the draft, and reviewed and edited the paper.

Conflicts of interest

There are no conflicts to declare.

Acknowledgements

This work is supported by the Natural Science Foundation of Jilin Province (20180101290JC) and the Fundamental Research Funds for the Central Universities.

References

- 1 K. Zeitler, *Angew. Chem., Int. Ed.*, 2009, **48**, 9785–9789.
- 2 J. Xuan and W.-J. Xiao, *Angew. Chem., Int. Ed.*, 2012, **51**, 6828–6838.
- 3 J. M. R. Narayanam and C. R. J. Stephenson, *Chem. Soc. Rev.*, 2011, **40**, 102–113.
- 4 R. A. Garza-Sanchez, A. Tlahuext-Aca, G. Tavakoli and F. Glorius, *ACS Catal.*, 2017, **7**, 4057–4061.
- 5 K. L. Skubi, T. R. Blum and T. P. Yoon, *Chem. Rev.*, 2016, **116**, 10035–10074.
- 6 D. Ravelli, M. Fagnoni and A. Albini, *Chem. Soc. Rev.*, 2013, **42**, 97–113.
- 7 T. P. Yoon, M. A. Ischay and J. Du, *Nat. Chem.*, 2010, **2**, 527–532.
- 8 C. K. Prier, D. A. Rankic and D. W. C. MacMillan, *Chem. Rev.*, 2013, **113**, 5322–5363.
- 9 H. Wang, X. Yang, W. Shao, S. Chen, J. Xie, X. Zhang, J. Wang and Y. Xie, *J. Am. Chem. Soc.*, 2015, **137**, 11376–11382.
- 10 H. Chen, C. Liu, M. Wang, C. Zhang, N. Luo, Y. Wang, H. Abroshan, G. Li and F. Wang, *ACS Catal.*, 2017, **7**, 3632–3638.
- 11 Y. Zhang, L. Pei, Z. Zheng, Y. Yuan, T. Xie, J. Yang, S. Chen, J. Wang, E. R. Waclawik and H. Zhu, *J. Mater. Chem. A*, 2015, **3**, 18045–18052.
- 12 X.-B. Li, Z.-J. Li, Y.-J. Gao, Q.-Y. Meng, S. Yu, R. G. Weiss, C.-H. Tung and L.-Z. Wu, *Angew. Chem., Int. Ed.*, 2014, **53**, 2085–2089.
- 13 L. Chen, J. Tang, L.-N. Song, P. Chen, J. He, C.-T. Au and S.-F. Yin, *Appl. Catal., B*, 2019, **242**, 379–388.
- 14 A. Casado-Sánchez, R. Gómez-Ballesteros, F. Tato, F. J. Soriano, G. Pascual-Coca, S. Cabrera and J. Alemán, *Chem. Commun.*, 2016, **52**, 9137–9140.
- 15 Z. Li, C. Liu, H. Abroshan, D. R. Kauffman and G. Li, *ACS Catal.*, 2017, **7**, 3368–3374.
- 16 N. Kang, J. H. Park, K. C. Ko, J. Chun, E. Kim, H.-W. Shin, S. M. Lee, H. J. Kim, T. K. Ahn, J. Y. Lee and S. U. Son, *Angew. Chem., Int. Ed.*, 2013, **52**, 6228–6232.
- 17 A. Talla, B. Driessen, N. J. W. Straathof, L.-G. Milroy, L. Brunsveld, V. Hessel and T. Noë, *Adv. Synth. Catal.*, 2015, **357**, 21801–21861.
- 18 M. Oba, K. Tanaka, K. Nishiyama and W. Ando, *J. Org. Chem.*, 2011, **76**, 4173–4177.
- 19 H. Li, F. Qin, Z. Yang, X. Cui, J. Wang and L. Zhang, *J. Am. Chem. Soc.*, 2017, **139**, 3513–3521.
- 20 Y. Qian, D. Li, Y. Han and H.-L. Jiang, *J. Am. Chem. Soc.*, 2020, **142**, 20763–20771.
- 21 S. Zhao, C. Liu, Y. Guo, J.-C. Xiao and Q.-Y. Chen, *J. Org. Chem.*, 2014, **79**, 8926–8931.
- 22 B. Chen, L. Wang, W. Dai, S. Shang, Y. Lv and S. Gao, *ACS Catal.*, 2015, **5**, 2788–2794.
- 23 S. L. James, *Chem. Soc. Rev.*, 2003, **32**, 276–288.
- 24 S. Kitagawa and R. K. S. Noro, *Angew. Chem.*, 2004, **116**, 2388–2430.
- 25 A. Dhakshinamoorthy, Z. Li and H. Garcia, *Chem. Soc. Rev.*, 2018, **47**, 8134–8172.
- 26 A. H. Chughtai, N. Ahmad, H. A. Younus, A. Laypkovc and F. Verpoort, *Chem. Soc. Rev.*, 2015, **44**, 6804–6849.

- 27 X. Liang, Z. Guo, H. Wei, X. Liu, H. Lv and H. Xing, *Chem. Commun.*, 2018, **54**, 13002–13005.
- 28 H. Wei, Z. Guo, X. Liang, P. Chen, H. Liu and H. Xing, *ACS Appl. Mater. Interfaces*, 2019, **11**, 3016–3023.
- 29 H. Liu, Z. Guo, H. Lv, X. Liu, Y. Che, Y. Mei, R. Bai, Y. Chi and H. Xing, *Inorg. Chem. Front.*, 2020, **7**, 1016–1025.
- 30 C. Xu, H. Liu, D. Li, J.-H. Sub and H.-L. Jiang, *Chem. Sci.*, 2018, **9**, 3152–3158.
- 31 D. Sun, L. Ye and Z. Li, *Appl. Catal., B*, 2015, **164**, 428–432.
- 32 S. Yuan, T.-F. Liu, D. Feng, J. Tian, K. Wang, J. Qin, Q. Zhang, Y.-P. Chen, M. Bosch, L. Zou, S. J. Teat, S. J. Dalgarno and H.-C. Zhou, *Chem. Sci.*, 2015, **6**, 3926–3930.
- 33 E. A. Dolgoplova, A. M. Rice, C. R. Martin and N. B. Shustova, *Chem. Soc. Rev.*, 2018, **47**, 4710–4728.
- 34 M. Li, G. Ren, W. Yang, Y. Yang, W. Yang, Y. Gao, P. Qiu and Q. Pan, *Chem. Commun.*, 2021, **57**, 1340–1343.
- 35 D. Gu, W. Yang, D. Lin, X. Qin, Y. Yang, F. Wang, Q. Pan and Z. Su, *J. Mater. Chem. C*, 2020, **8**, 13648–13654.
- 36 V. Guillerme, Ł. J. Weseliński, Y. Belmabkhout, A. J. Cairns, V. D'Elia, Ł. Wojtas, K. Adil and M. Eddaoudi, *Nat. Chem.*, 2014, **6**, 673–680.
- 37 J. Liu, D. Wu, G.-P. Yang, Y. Wu, S. Zhang, J. Jin and Y.-Y. Wang, *Chem. – Eur. J.*, 2020, **26**, 5400–5406.
- 38 S. M. Hawxwell and L. Brammer, *CrystEngComm*, 2006, **8**, 473–476.
- 39 H. F. Clausen, R. D. Poulsen, A. D. Bond, M.-A. S. Chevallier and B. B. Iversen, *J. Solid State Chem.*, 2005, **178**, 3342–3351.
- 40 Q.-H. Tan, Y.-Q. Wang, X.-Y. Guo, H.-T. Liu and Z.-L. Liu, *RSC Adv.*, 2016, **6**, 61725–61731.
- 41 J. Xu, J. Cheng, W. Su and M. Hong, *Cryst. Growth Des.*, 2011, **11**, 2294–2301.
- 42 V. Zelenák, Z. Vargová and K. Györyová, *Spectrochim. Acta, Part A*, 2007, **66**, 262–272.
- 43 C. Falaise, C. Volkringer and T. Loiseau, *Cryst. Growth Des.*, 2013, **13**, 3225–3231.
- 44 C. H. Hendon, D. Tiana, M. Fontecave, C. Sanchez, L. D'arras, C. Sassoie, L. Rozes, C. Mellot-Draznieks and A. Walsh, *J. Am. Chem. Soc.*, 2013, **135**, 10942–10945.
- 45 M. T. Schümperli, C. Hammond and I. Hermans, *ACS Catal.*, 2012, **2**, 1108–1117.
- 46 L. M. Aguirre-Díaz, N. Snejko, M. Iglesias, F. Sánchez, E. Gutiérrez-Puebla and M. A. Monge, *Inorg. Chem.*, 2018, **57**, 6883–6892.
- 47 Y. Sha, J. Zhang, D. Tan, F. Zhang, X. Cheng, X. Tan, B. Zhang, B. Han, L. Zheng and J. Zhang, *Chem. Commun.*, 2020, **56**, 10754–10757.
- 48 J. Shi, J. Zhang, T. Liang, D. Tan, X. Tan, Q. Wan, X. Cheng, B. Zhang, B. Han, L. Liu, F. Zhang and G. Chen, *ACS Appl. Mater. Interfaces*, 2019, **11**, 30953–30958.
- 49 R. Liu, S. Meng, Y. Ma, L. Niu, S. He, X. Xu, B. Su, D. Lu, Z. Yang and Z. Lei, *Catal. Commun.*, 2019, **124**, 108–112.
- 50 X. Liu, B. Liu, G. Li and Y. Liu, *J. Mater. Chem. A*, 2018, **6**, 17177–17185.
- 51 Q. Xia, X. Yu, H. Zhao, S. Wang, H. Wang, Z. Guo and H. Xing, *Cryst. Growth Des.*, 2017, **17**, 4189–4195.
- 52 Y. Zhang, S. Liu, Z.-S. Zhao, Z. Wang, R. Zhang, L. Liu and Z.-B. Han, *Inorg. Chem. Front.*, 2021, **8**, 590–619.
- 53 F. Wang, Y. Pu, X. Zhang, F. Zhang, H. Cheng and Y. Zhao, *J. Lumin.*, 2019, **206**, 192–198.
- 54 X. Deng, J. Albero, L. Xu, H. García and Z. Li, *Inorg. Chem.*, 2018, **57**, 8276–8286.
- 55 Z.-H. Yan, M.-H. Du, J. Liu, S. Jin, C. Wang, G.-L. Zhuang, X.-J. Kong, L.-S. Long and L.-S. Zheng, *Nat. Commun.*, 2018, **9**, 3353–3361.
- 56 X. Lian and B. Yan, *Inorg. Chem.*, 2016, **55**, 11831–11838.
- 57 R. W. Gable, L. Hou, S. R. B. K. Gelderman, L. Lee and S. W. Donne, *J. Chem. Educ.*, 2007, **84**, 685–688.
- 58 H.-Q. Xu, J. Hu, D. Wang, Z. Li, Q. Zhang, Y. Luo, S.-H. Yu and H.-L. Jiang, *J. Am. Chem. Soc.*, 2015, **137**, 13440–13443.
- 59 B. E. Block, *Angew. Chem., Int. Ed. Engl.*, 1992, **31**, 1135–1178.
- 60 Y. Kanda and T. Fukuyama, *J. Am. Chem. Soc.*, 1993, **115**, 8451–8452.
- 61 K. Y. D. Tan, G. F. Teng and W. Y. Fan, *Organometallics*, 2011, **30**, 4136–4143.
- 62 D. H. Scharf, M. Groll, A. Habel, T. Heinekamp, C. Hertweck, A. A. Brakhage and E. M. Huber, *Angew. Chem., Int. Ed.*, 2014, **53**, 2221–2224.
- 63 H. T. Abdel-Mohsen, K. Sudheendran, J. Conrad and U. Beifuss, *Green Chem.*, 2013, **15**, 1490–1495.
- 64 A. Shaabani, A. Bazgir and D. G. Lee, *Synth. Commun.*, 2004, **35**, 3595–3607.
- 65 M. Bagheri, N. Azizi and M. R. Saidi, *Can. J. Chem.*, 2005, **83**, 146–149.
- 66 N. Iranpoor and B. Zeynizadeh, *Synthesis*, 1999, 49–50.
- 67 S. Ghammamy and M. Tajbakhsh, *J. Sulfur Chem.*, 2005, **26**, 145–148.
- 68 M. A. Walters, J. Chaparro, T. Siddiqui, F. Williams, C. Ulku and A. L. Rheingold, *Inorg. Chim. Acta*, 2006, **359**, 3996–4000.
- 69 H. Huang, J. Asha and J. Y. Kang, *Org. Biomol. Chem.*, 2018, **16**, 4236–4242.
- 70 J. L. G. Ruano, A. Parra and J. Alemán, *Green Chem.*, 2008, **10**, 706–711.
- 71 E. L. Tyson, Z. L. Niemeyer and T. P. Yoon, *J. Org. Chem.*, 2014, **79**, 1427–1436.
- 72 T. Miyashita and M. Matsuda, *Bull. Chem. Soc. Jpn.*, 1981, **54**, 1740–1742.
- 73 M. H. V. Huynh and T. J. Meyer, *Chem. Rev.*, 2007, **107**, 5004–5064.
- 74 A. Adenier, M. M. Chehimi, I. Gallardo, J. Pinson and N. Vilà, *Langmuir*, 2004, **20**, 8243–8253.
- 75 C. K. Mann, *Anal. Chem.*, 1964, **36**, 2424–2426.
- 76 E. L. Tyson, M. S. Ament and T. P. Yoon, *J. Org. Chem.*, 2013, **78**, 2046–2050.
- 77 F. G. Bordwell, X.-M. Zhang, A. V. Satish and J.-P. Cheng, *J. Am. Chem. Soc.*, 1994, **116**, 6605–6610.